Proceedings of the Society for

EXPERIMENTAL MECHANICS, INC.

Proceedings of the Society for

EXPERIMENTAL MECHANICS, INC.

(Formerly the Society for Experimental Stress Analysis)

VOLUME XLIII

K.A. Galione, Publisher
M.E. Yergin, Managing Editor

THE SOCIETY FOR EXPERIMENTAL MECHANICS, INC.

The Society for Experimental Mechanics, Inc. (formerly the Society for Experimental Stress Analysis) was founded in 1943 as a non-profit scientific and educational organization. Its objective is to "promote and encourage the furtherance of knowledge pertaining to experimental mechanics."

The members of SEM represent a unique network of leaders in experimental mechanics in the U.S. and abroad. They are active in academia, government and industrial research and development and include scientists, engineers, manufacturers, consultants, users and vendors of plant equipment, services and systems. SEM also maintains close contact with other professional groups throughout the world with cooperative meetings and joint membership options.

SEM is large enough to have a broad base in mechanics, yet small enough to maintain good communication between members with diverse specialties. The Technical Divisions within SEM offer interdisciplinary lines of communication and include several professional interests in Composite Materials, Fracture, Modal Analysis/Dynamic Systems, Structural Testing, Residual Stress, Optical Methods, Strain Gages, Transducers and Applied Photoelasticity. Local section meetings provide opportunities for members to meet regularly and exchange information and enjoy professional as well as social contact.

SEM sponsors Spring and Fall Conferences with exhibits, co-sponsors the International Conference on Modal Analysis (IMAC) with Union College, topical conferences and educational seminars. These, along with the monthly magazine, EXPERIMENTAL TECHNIQUES, and the quarterly journals EXPERIMENTAL MECHANICS and the INTERNATIONAL JOURNAL OF ANALYTICAL AND EXPERIMENTAL MODAL ANALYSIS, serve to meet the objectives of the Society. A comprehensive collection of technical literature is available from SEM's publication department.

For membership information contact SEM, 7 School Street, Bethel, CT 06801. (203) 790-6373.

NOTE: The opinions expressed on the following pages are those of the individual authors and do not necessarily represent the ideas of the Society for Experimental Mechanics, Inc.

Proceedings of the Society for Experimental Mechanics, Inc.*

*In 1984, the Society officially changed its name from "Society for Experimental Stress Analysis" to "Society for Experimental Mechanics." Due to a bookbinding error, Vol. 42 (1985) was bound under the former name "Society for Experimental Stress Analysis."

Contents

A Laser-Interferometric Dilatometer for Thermal-Expansion Measurements of Composites

by S.S. Tompkins, D.E. Bowles and W.R. Kennedy

ABSTRACT—A high-precision, Fizeau-type laser-interferometric dilatometer system has been developed for low-expansion composite materials. The strain resolution is about one microstrain. The system is automated to operate over a large temperature range and record data during the test. A technique has been developed to reduce the data in real time. The dilatometer system is described and thermal-expansion measurements for several fiber-reinforced and particle-filled composites are presented.

Introduction

Precision space structures that have very strict tolerances on dimensional control require materials that possess a high specific stiffness and a low coefficient of thermal expansion. Graphite-reinforced composites meet both of these requirements and are currently being used for such structures as well as planned for use in future space structures. The space environment includes high vacuum, radiation, and thermal cycling. Temperature extremes may be as low as 115 °K and as high as 422 °K. In order to characterize the dimensional stability of composites subjected to this service environment, a method to measure thermal strains on the order of 1 to 10 $\times$ 10^{-6} is needed.

A comprehensive survey and discussion of available techniques to measure small displacements are given in Refs. 1 and 2. These techniques can be divided into three categories: electromechanical, optical noninterferometric and optical interferometric. The application of electromechanical techniques, such as the push-rod dilatometer and strain gages, to composites is discussed in Ref. 3. The measurement of the ultra-small displacements, such as those associated with high dimensionally stable materials, requires the resolution achievable with the interferometric techniques. The application of two of these techniques, the Michelson and moiré interferometers, to composites is discussed in Refs. 4 and 5 respectively.

There are several important requirements for a measurement technique for low-expansion composites. The technique must be capable of using composite specimens long enough to minimize edge effects and the effects of local inhomogenities. For example, specimens with chamfered ends must be two in. or longer to keep the induced error in the coefficient of thermal expansion, due to end effects, below one percent (Ref. 6). Also, the technique should be capable of measuring a wide range of expansion as well as a variety of specimen configurations. Specimen preparation must be minimal because the material must be characterized both after and during exposure to environmental parameters. A technique based upon Fizeau interferometry has been developed that meets all of these requirements.

This paper describes a system developed at the NASA Langley Research Center to characterize and study the expansion behavior of composites and low-expansion materials. The salient features of the system include: (1) high precision, (2) automated data acquisition, and (3) capability to test a wide variety of specimen geometries over the temperature range 89 °K to 422 °K. Although this system has been operated only at atmospheric pressure, the basic design can easily be adapted to measurements in vacuum.

Theory of Operation

A Fizeau-type interferometer was selected for the current application. This type of interferometer measures

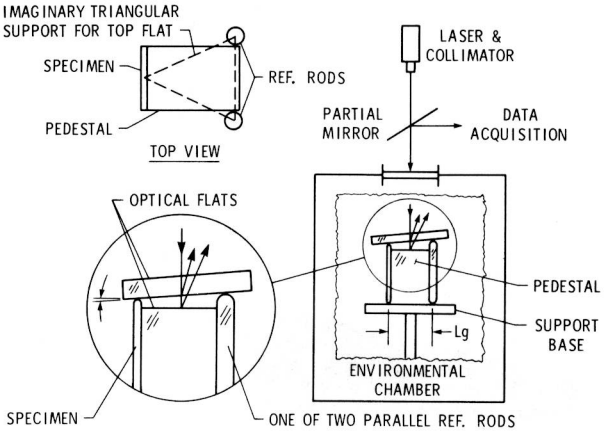

Fig. 1—Schematic diagram for Fizeau-type interferometer

S.S. Tompkins (SEM Member) is Senior Materials Researcher and D.E. Bowles (SEM Member) is Materials Research Engineer, NASA Langley Research Center, Hampton, VA 23665. W.R. Kennedy (SEM Member) is Project Engineer, Kentron International, Inc., 3221 North Armistead Avenue, Hampton, VA 23665.

Paper was presented at V International Congress on Experimental Mechanics held in Montreal, Quebec, Canada on June 10-15, 1984.

Original manuscript submitted: December 15, 1984. Final manuscript received: July 29, 1985.

the change in length of a test specimen relative to the change in length of a known material. The application of Fizeau interferometry to measure thermal expansion is described in Ref. 7. The type of Fizeau interferometer used in this development is discussed in Refs. 8-10 and a brief description is given here for completeness.

A schematic diagram of the interferometer is shown in Fig. 1 and the components and assembled interferometer are shown in Fig. 2. The specimen and two rods of a reference material are oriented vertically. The two reference rods are located on the opposite side of a pedestal from the specimen and form a triangle with the specimen on which an optical flat is supported (Fig. 1). The base, pedestal and the optical flat are made with an ultra-low-expansion glass and the base and pedestal are joined by optical contact. The pedestal and a mechanical spring system are used to maintain both the specimen and reference rods in a vertical position [Fig. 2(b)]. The lengths of the reference rods are about the same but different from the specimen length which result in a small angle, θ, between the two flats (Fig. 1). The incident laser beam reflects from the top and bottom surfaces of the top flat and from the top of the pedestal. The top surface of the top flat is slightly inclined to deflect unwanted reflections away from the incident beam. The reflections from the bottom of the top flat and the pedestal form an interference pattern which consists of a series of parallel fringes. The number of fringes over the gage length, Lg, is directly proportional to θ (Fig. 1). As the lengths of the reference rods and/or specimen change, the angle θ will also change. The change in θ is given by:

$$\Delta\theta = \frac{\Delta n \lambda}{2Lg} \tag{1}$$

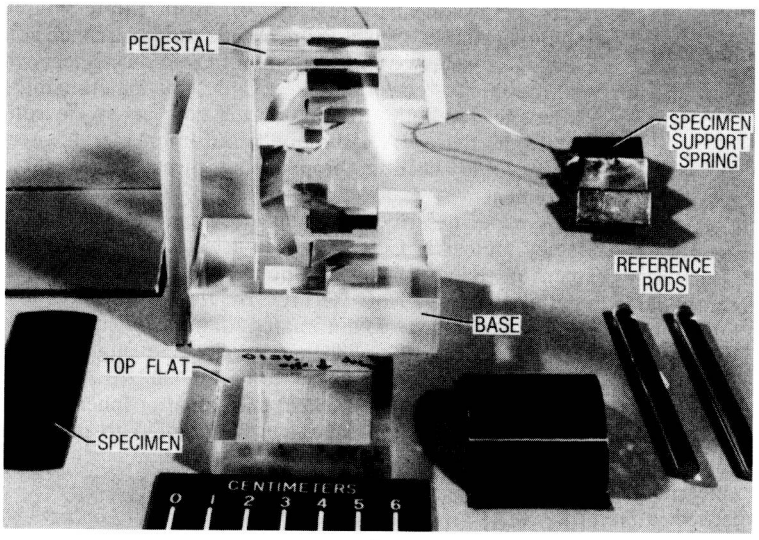

(a)

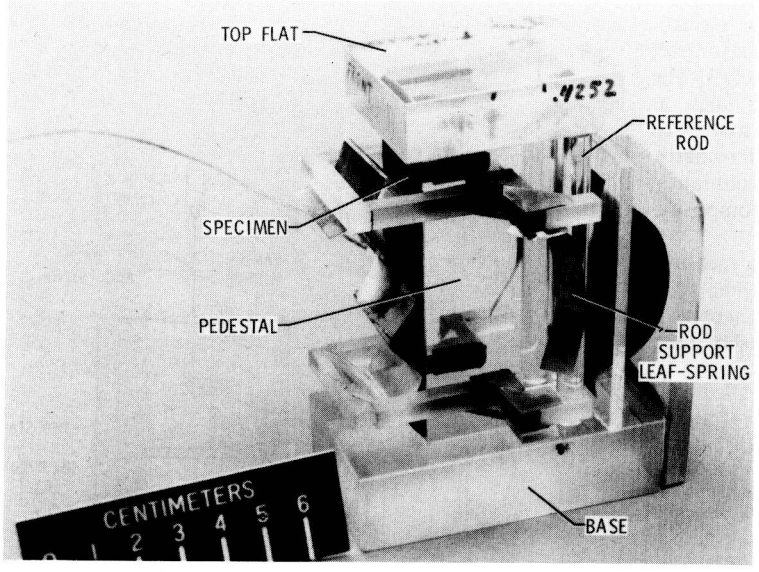

(b)

Fig. 2—Fizeau-type interferometer;
(a) exploded view of interferometer;
(b) assembled interferometer with specimen

where Δn is the change in the fringe count over the gage length, Lg, and λ is the laser wavelength. The relative strain, ϵ_r, for $\theta \ll 1$ deg, for a specimen of length L_s, is given by:

$$\epsilon_r = \frac{\Delta n \lambda}{2L_s} = \frac{\Delta N \lambda Lg}{2L_s} \tag{2}$$

where ΔN is the change in fringe density (fringes/cm). Since the thermal expansion of the reference, ϵ_R, is known, the total strain of the specimen, ϵ_I, is given by:

$$\epsilon_I = \epsilon_r + \epsilon_R \tag{3}$$

The interferometer can accommodate almost any length specimen if the pedestal height and reference rod lengths are adjusted. The pedestal is not required if the specimen could be supported another way and the base used as the second optical flat.

Experimental Method

Test System

A schematic diagram of the system developed to measure the dilation of low-expansion materials is shown in Fig. 3. The initial development of this system is reported in Ref. 8. Since the initial development, many improvements have been made. The system consists of: (1) an improved type of interferometry, (2) an environmental chamber, (3) an improved optical train, (4) a He-Ne laser, and (5) a camera. A photodiode array, a wave analyzer, and a computer have been added to automate the testing and data processing. The environmental chamber is controlled by the computer which also activates the camera and records test temperatures. The photodiode array and wave analyzer have been integrated into the system; calibration of the wave analyzer is in progress. The photodiode array and wave analyzer become the primary method for data acquisition and real-time data reduction and the camera becomes an alternate data-acquisition method. The data presented in this paper, except as noted, were recorded on camera and manually reduced.

The environmental chamber is an air-circulating, insulated chamber which can operate between 89 °K and 700 °K. The chamber is heated with resistance heaters and cooled by liquid nitrogen. The optical train consists of various lenses, a beam splitter, collimator, and several mirrors which provide a collimated monochromatic source for the interferometer, and which image the resulting fringe pattern onto both the photodiode array and camera. A 5-mW, He-Ne laser ($\lambda = 632.5 \times 10^{-9}$ m) is used for the light source.

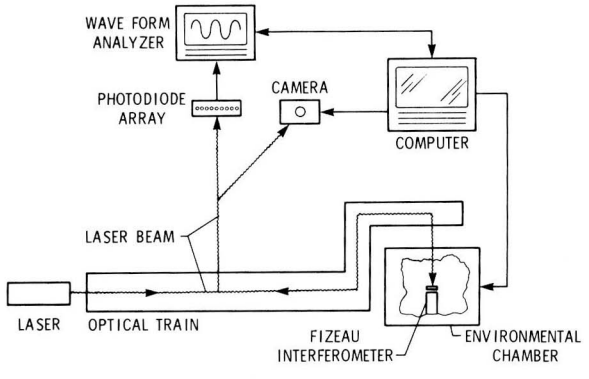

Fig. 3—Schematic diagram of the laser-interferometric dilatometer system

The fringe pattern is recorded at specified time intervals on 35-mm film or analyzed by a wave analyzer via a linear photodiode array with 403 light-sensitive silicon photodiodes per cm. The chamber temperature, data acquisition and test time are controlled by a microcomputer. The test-specimen temperature is monitored by a calibrated 30-gage Chromel-Alumel thermocouple in contact with the specimen. All thermocouples used in this study were calibrated using the NBS procedure G-44084. The maximum differences between the thermocouples and the standards were ±0.1 °K over the range of 297 °K to 422 °K. At 78 °K, the difference between thermocouples and the standard was about 3 °K. Thermocouple output was converted to temperature using the polynomial described in NBS Monograph 126. Correction tables were not used. Temperature surveys of the chamber, using matched thermocouples, have shown that 45 minutes after the temperature was changed, the temperature gradient along the length of a polymer composite specimen was approximately zero. The temperature gradient along the length of the NBS SRM 739 quartz reference rods was less than 0.2 °K/cm above room temperature and about 0.4 °K/cm below room temperature. The maximum difference between the average temperatures of the specimen and reference rods over the temperature range 117 °K to 422 °K was about 1 °K.

Test Procedure

Sample preparation is an important first step in the test procedure. Specimens are first machined to final length with the ends rounded or beveled to provide single-point contact with both the top flat and interferometer base [Fig. 2(b)]. The geometries of some of the specimens that have been successfully tested are shown in Fig. 4. After machining, all polymer composite-material samples are dried at 328 °K in vacuum to constant weight. This drying avoids any length change or permanent set due to absorption or 'desorption' of moisture. The surfaces of the interferometer in contact with the reference rods and specimens are thoroughly cleaned with alcohol before each test.

The cleaned interferometer with reference rods and specimen is placed in the chamber and the test is started. The initial fringe data are taken after the chamber has equilibrated. The setpoint on the temperature controller is changed in 22 °K steps every 45 minutes and data are taken at the end of each step. The rate of specimen temperature change never exceeds 1.7 °K per minute.

The measurement of specimen length change resulting from some environmental conditioning, for example several hundred thermal cycles, can also be made using this test apparatus without having to keep the specimen in the fixture during cycling. For this approach, the initial and final lengths of a sample are measured with the interferometer. That is, the initial fringe density is determined, then the sample is removed and cycled a specified amount, reinserted in the interferometer, and the final length is measured. Tests at room temperature have indicated that the samples can be reinserted into the interferometer with no more than four-microstrain difference.

Data Acquisition and Reduction

Two methods are currently used for recording and analyzing interference-fringe data. In the first method, individual fringe patterns are recorded on 35-mm film. At the conclusion of a test, the 35-mm negatives are enlarged in a microfiche reader and the number of fringes are visually counted over a defined length. The fringe density is then simply the number of fringes divided by the length over which they are counted. The film also serves as a permanent record of the data for a given test.

The second method allows fringe patterns to be analyzed in real time. The fringe pattern is imaged onto a light-sensitive linear photodiode array. The photodiode array is electrically scanned and the fringe pattern is digitized. The digitized signal, which has a sinusoidal form [Fig. 5(a)], is then transmitted to a waveform analyzer. The waveform analyzer performs a fast-Fourier transform (FFT) on the signal to determine the temporal-frequency content. Details of the FFT analysis to determine frequency content may be found in Ref. 11. The FFT for the signal shown in Fig. 5(a) is given in Fig. 5(b). The predominant frequency in the signal is the sine-wave frequency, from which the fringe density can be directly computed as follows.

$$N = \frac{F_s\, t_{scan}}{L_{pd}} \qquad (4)$$

where N is the fringe density, F_s is the sine frequency, t_{scan} is the scan time and L_{pd} is the length displayed on the photodiode array.

For fringe densities in the range of 0.4 to 39 fringes/cm gage length, the frequency range is approximately 20 to 2000 Hz. The above procedure is completely automated and controlled by the computer such that fringe densities are computed in real time. Fringe densities computed from the FFT analysis have been found to be in good agreement with fringe densities computed from the film, as will be discussed in a subsequent section.

The change in fringe density, ΔN, is used in eq (2) to calculate the relative thermal strain between the specimen and reference rods and the total strain of the specimen is then determined with eq (3). The thermal-strain data for NBS SRM 739 fused silica, used in this study, were taken from the NBS Certificate of Analysis supplied with the SRM 739 rods.

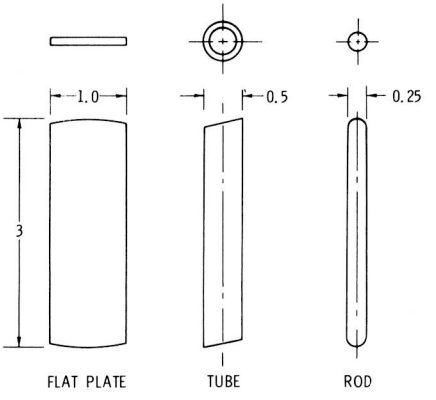

Fig. 4—Typical specimen sizes and geometries used in Fizeau-type interferometer, dimensions in centimeters

The strain resolution attainable with the current interferometer is directly related to the precision with which the fringe density can be determined. For the film, this corresponds to how accurately the number of fringes, over the gage length Lg, can be counted. The current technique yields data to the nearest ¼ fringe which results in a strain resolution of approximately one microstrain. It should be noted that this fringe resolution is a function of the total number of fringes. For a low number of fringes, less than ten, the fringe count can be determined to at least the nearest 1/10 fringe. However, for a large number of fringes, greater than 100, the fringe resolution may be as low as ½ fringe. Therefore, the total number of fringes should be kept as low as possible. This is accomplished by using reference rods with a thermal expansion as close as possible to that of the specimen.

Results and Discussion

Fused Silica and Invar

The precision of the measurement technique was established by repeated tests of the same specimen for both NBS SRM 739 fused silica and Invar. All of these tests were run using NBS SRM 739 as the reference material. Data from these tests were collected on film and analyzed as previously described. All of the data were adjusted to zero strain at 293 °K.

Data from four tests, a total of 103 data points, were collected on a sample of NBS SRM 739 fused silica and are plotted in Fig. 6. Ideally, the relative strain, ϵ_r, for these tests should be zero, i.e., the total strain equal to the strain of the reference material [eq (3)]. This is because both the sample and reference are the same material. However, as shown in Fig. 6, there are some small

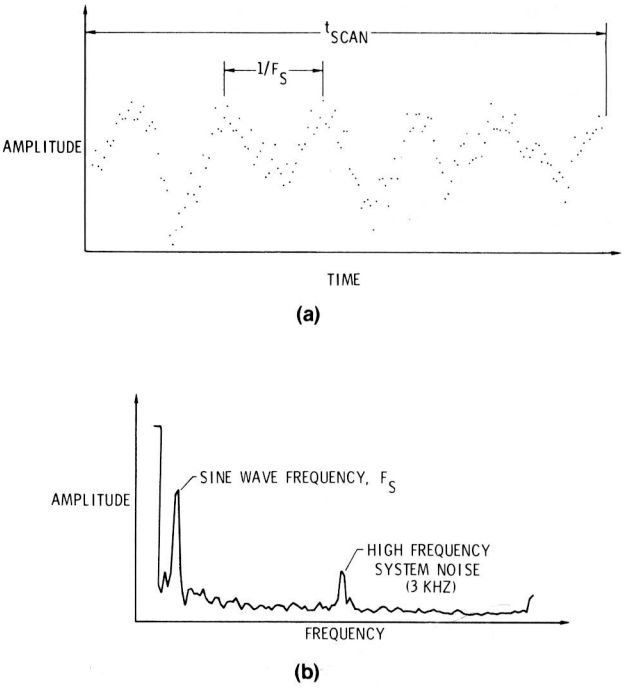

Fig. 5—Typical digitized fringe pattern and fast-Fourier transform of digitized fringe pattern; (a) digitized fringe pattern; (b) fast-Fourier transform of digitized fringe pattern

differences between the total strain and the strain of the reference. These may be attributed to the variability of the thermal expansion of the material used in the reference and sample. A root-mean-square (RMS) error for this data was computed from the following:

$$\text{RMS} = \sqrt{\frac{\sum_{i=1}^{M} (y_i - \hat{y}_i)^2}{M}} \qquad (5)$$

where y_i is the measured value, $\hat{y}_i$ is the predicted value, and M is the total number of data points. The RMS error for the fused-silica data, using the fourth-order polynomial supplied by NBS for the thermal expansion of fused silica as $\hat{y}_i$, was 0.80 microstrain.

Data were also collected from seven tests—a total of 191 data points—of an annealed Invar 36 sample. These data, together with a fourth-order least-squares polynomial fit to the data, are shown in Fig. 7. The RMS error for this data, using the polynomial fit as $\hat{y}$ in eq (5), is 2.67 microstrain. The larger scatter for the Invar data as compared to the fused-silica data (2.67 microstrain compared to 0.80 microstrain) is, for the most part, attributed to the high-fringe densities in the Invar tests due to the large difference in expansion coefficients of the Invar and fused silica. As previously stated, the resolution, and therefore the precision, decreases, at high-fringe densities. Maximum-fringe densities for the Invar tests were about 28 fringes/cm compared to about 1 fringe/cm for the fused silica. Data from both the fused silica and Invar indicate a precision for the current interferometer in the range of about one to three microstrain.

A comparison of data computed from the film and from the FFT analysis is shown in Fig. 8. The data shown are for one test of the Invar specimen. The two sets of data are in good agreement, with a maximum difference of 4.7 microstrain. The majority of this difference is caused by a misalignment of the fringe-pattern image on the photodiode array. A method to more accurately align the fringe pattern on the photodiode array is currently under development.

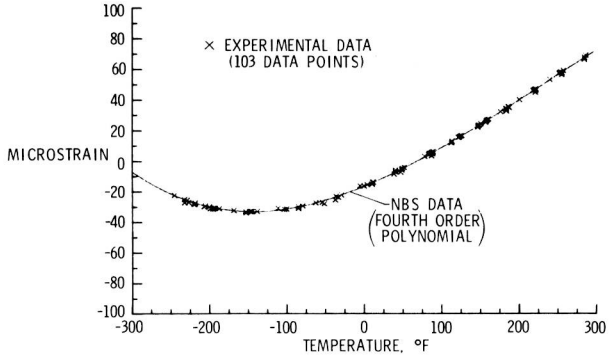

Fig. 6—Thermal expansion data for NBS SRM 739 fused silica

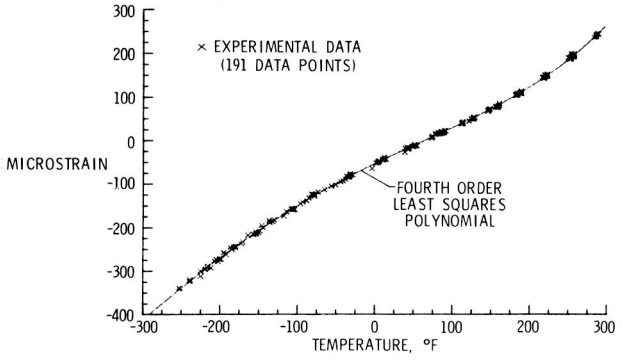

Fig. 7—Thermal expansion data for Invar 36

Composites

The application of the present dilatometer system to define and understand the response of materials to their service environment is illustrated in Figs. 9-11. These measurements also illustrate the capabilities of this system. All of the samples tested were composites, each about 7.6-cm long. The expansions of the continuous fiber-reinforced composites were made in the 0-deg fiber direction.

Data that characterize the expansion of the baseline material are often the first type of data needed. This type of data over the temperature range of 117 °K to 394 °K is shown in Fig. 9 for different laminates of a graphite/polyimide composite, C6000/PMR-15, composed of Celion 6000 graphite fibers (Celanese Corporation) and PMR-15 polyimide resin. The total expansion of a unidirectional laminate is nonlinear and relatively small, about 80 microstrain, over the temperature range. This behavior is very different from the expansion of a quasi-isotropic laminate, $[0/\pm 45/90]_s$. The total expansion of the latter is about 475 microstrain over the same temperature range and is slightly nonlinear with temperature.

If a material is subjected to thermal cycling in its service environment, the response of the material during these cycles must be defined and understood. The present dilatometer system allows expansion measurements to be made, *in situ*, during continuous thermal cycling. An example of this is shown in Fig. 10 where data are shown for a metal-matrix composite material, 6061 aluminum reinforced with Union Carbide P100 carbon fibers, continuously cycled up to ten times between 117 °K and 394 °K. The expansion during these cycles is characterized by a large hysteresis loop, which becomes smaller as the material is cycled but does not close. After the first cycle, the specimen had shrunk about 40 microstrain,

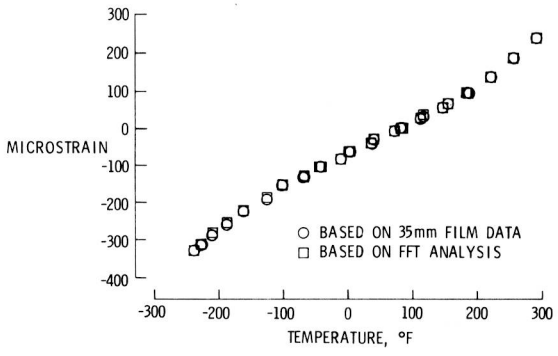

Fig. 8—Thermal expansion data for Invar computed from fringe densities determined from 35-mm film and photodiode array with fast-Fourier-transform (FFT) analysis

but returned to its original length after the tenth cycle. The expansion behavior of this material is attributed to elastic/plastic deformation within the composite caused by large internal thermal stresses. These stresses result from the large difference between the coefficients of thermal expansion of the matrix and the fiber reinforcement.

One advantage of a relative-measurement technique is to directly compare the expansion of two materials. Aerodynamic models, especially those used in wind tunnels where the boundary layers are thin, must have very smooth surfaces. Even a small disturbance from the expansion of a hole-filler material, used on the model, into the boundary layer is undesirable. A hole-filler material was needed for models to be tested in the new NASA National Transonic Facility at LaRC. Thermal-expansion data for two particle-filled composites proposed for filler material are shown in Fig. 11. This type of data is being used to determine the mix of 190-micron solid carbon spheres and Hysol 9309 epoxy resin required to match the expansion of 6061 aluminum, the material used for the aerodynamic models. The data also emphasize the sensitivity of thermal expansion of a composite to composition.

Concluding Remarks

A high-precision, Fizeau-type laser-interferometric dilatometer system has been developed to characterize low-expansion composite materials. The strain resolution is about one microstrain. Specimens with a variety of geometries have been used and the system can be modified to measure specimens of almost any length. The system is automated to operate over a large temperature range unattended and record data during the test with a camera. A technique has been developed and is being calibrated to reduce the fringe data, in real time, to length changes. With this technique, the light-dark fringe pattern detected by a photodiode array is analyzed with a fast-Fourier transform from which the fringe density, and subsequently the length change, is calculated. Thermal-expansion measurements have been made on several fiber-reinforced and particle-filled composites. These include *in situ* measurements during thermal cycling.

Acknowledgments

The authors wish to acknowledge Cheri L. Wood, NASA-Langley Research Center, who conducted many of the tests and reduced much of the data presented in this paper.

References

1. Wolff, E., Measurement Techniques for Low Expansion Materials, **9**, *Nat. SAMPE Tech. Conf. Series (Oct. 1977).*

2. Johnson, R.R., Kural, M.H. and Mackey, G.B., Thermal Expansion Properties of Composite Materials, NASA CR165632 (July 1981).

3. Freeman, W.T. and Campbell, M.D., "Thermal Expansion Characteristics of Graphite Reinforced Composite Materials," Composite Materials: Testing and Design, ASTM STP 497, 121-142 (1972).

4. Eselun, S.A., Neubert, H.D. and Wolff, E.G., Microcracking Effects on Dimensional Stability, **24**, *SAMPE Tech. Conf. Series (May 1979).*

5. Bowles, D.E., Post, D., Herakovich, C.T. and Tenney, D.R., "Moiré Interferometry for Thermal Expansion of Composites," EXPERIMENTAL MECHANICS, **21** *(12), 441-448 (Dec. 1981).*

6. Kural, M.H. and Ellison, A.M., "Induced Errors During Thermal Expansion Testing of Graphite Fiber Reinforced Metal Matrix Composites," SAMPE J., 20-26 (Sept.-Oct. 1980).

7. ASTM Standard Test Method for "Linear Thermal Expansion of Rigid Solids with Interferometry," Designated E289, 1982 Annual Book of ASTM Standards, Part 41, 316-323.

8. Short, J.S., Hyer, M.W., Post, D., Bowles, D.E. and Tompkins, S.S., Development of a Priest Interferometer for Measurement of the Thermal Expansion of Graphite-Epoxy in the Temperature Range, 116-366K, VPI-E-82-18 Dept. of Eng. Sci. and Mech., VPI & SU (Sept. 1982).

9. Plummer, W.A. and Hagy, H.E., A High Precision Priest Interferometer, 6th Therm. Expans., Proc. Int. Symp., ed. Peggs and Plenum, 173-186 (1977).

10. Hyer, M.W., Herakovich, C.T. and Post, D., "Thermal Expansion of Graphite Epoxy," 1982 Advances in Aerospace Structures and Materials, AD-03, ed. R.M. Laurenson and U. Yuceoglu, ASME, 107-113.

11. Weaver, J.H., Applications of Discrete and Continuous Fourier Analysis, John Wiley & Sons, Inc. (1983).

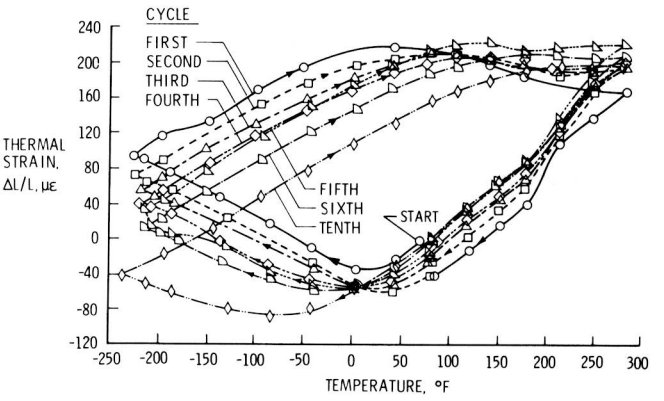

Fig. 10—Thermal expansion data for P100/6061, a graphite-aluminum composite, during ten continuous thermal cycles

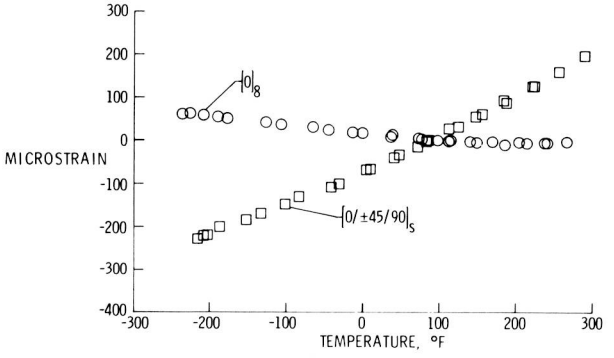

Fig. 9—Thermal expansion of a quasi-isotropic and a unidirectional laminate of C6000/PMR-15 graphite-polyimide composite

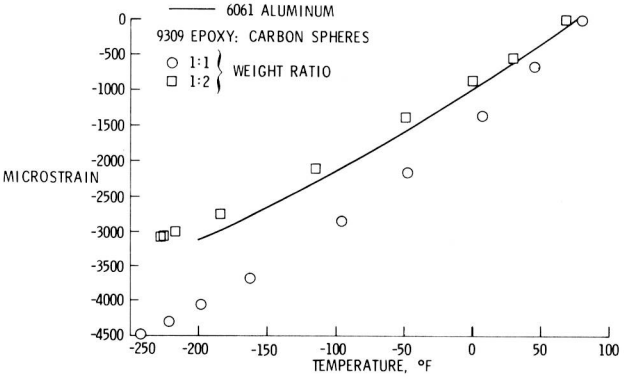

Fig. 11—Thermal expansion of a carbon-filled 9309 epoxy resin compared to 6061 aluminum

A Review: Acoustic Emission, a Tool for Composite-Materials Studies

by Marvin A. Hamstad

ABSTRACT—The technique of acoustic emission has two broad applications areas. The first is nondestructive evaluation. The second is as a tool in studies or research which are not fundamentally directed towards acoustic emission. It is this second application with which we are concerned here. Acoustic emission is a very useful tool in this role because of its high sensitivity, real-time capability, volume-monitoring approach, and sensitivity to any process or mechanism which generates sound waves. This paper presents a comprehensive review of areas where acoustic emission (AE) has been used for materials studies on composite materials. The following fields, among others, will be covered: (1) time-dependent composite properties, (2) impact studies, (3) correlation of AE with stress level, (4) application to matrix cure studies, (5) relationship of AE-detected damage to other measures of damage, (6) studies of the effects of matrix material, (7) application to differences in second phase, (8) interface studies, (9) AE and dimensional stability, (10) AE applied to orientation studies, and (11) environmental effects. This review will emphasize the roles that AE can play as a tool for the materials scientist: (1) discovery of damage mechanisms, (2) characterization of damage progression with increasing time or stress, (3) optimization of fabrication variables, and (4) reduction in the numbers of test specimens required in various studies.

Introduction

Composite materials under stress experience numerous damage mechanisms. For example, these may include fiber or second-phase failure, delamination, matrix cracking, debonding of phases, etc. These damage mechanisms can occur at numerous locations throughout a composite beginning at very low stress levels. The task of keeping track of all of these damage sites and mechanisms is far more complex than simply monitoring crack growth at a few locations in a metallic material. Because the accumulation of damage in a composite is closely tied to the actual strength, life and stiffness of the composite, understanding the development of this damage is very important to the materials scientist and engineer who use composite materials for structural applications.

Several methods have been used to monitor the damage occurrences in composites. Among these the technique of acoustic emission (AE) has been increasingly used. AE is based on monitoring the stress waves that are generated by rapid local redistributions of stress which accompany the operation of many damage mechanisms. Pointing to the growth of the use of AE for materials studies is the fact that over 500 papers or reports have been published in this area since 1970. AE offers a number of advantages and potential advantages which give the technique some unique capabilities. Among these are: (1) high sensitivity, (2) real-time capability, (3) total specimen volume sensitivity, (4) location of damage regions, and (5) sensitivity to any process or mechanism that generates stress waves.

The goal of this paper is to present a comprehensive review of areas where AE has been used for materials studies. Comprehensive does not mean that all such publications will be considered. Instead, the attempt will be to cover the general areas where AE has been used with typical examples. Further references may be found in either of two extensive bibliographies.[1,2]

Survey of Applications

Application to Time-Dependent Studies

Rotem and Baruch[3] used AE monitoring to characterize damage accumulation as a function of time in unidirectional glass/epoxy samples under load holds. They also used AE to characterize damage which occurred with proof cycles interspersed during the load holds. Rotem[4] shows by AE that the damage during a tensile test of unidirectional E-glass/epoxy depended on the strain rate. He observed an increase in the number of AE events when the strain rate decreased (see Fig. 1). He notes that these strain-rate effects did not occur with graphite fibers in the same epoxy. Ryder and Wadin[5] used AE to track the initiation of damage and the progression of damage in graphite/epoxy laminates during tension-tension fatigue testing. Eisenblatter *et al.*[6] show during fatigue of glass-reinforced composites that the damage growth as characterized by the summation of counts showed high rates of damage for the early fatigue

Marvin A. Hamstad (SEM Member) is Professor of Mechanical Engineering, Department of Engineering, University of Denver, Denver, CO 80208.

Original manuscript submitted: April 15, 1985. Final manuscript received: August 1, 1985.

cycles and the fatigue cycles near failure. Between the beginning and the end, the damage rate was much lower. Fuwa *et al.*[7] compare damage progression in graphite/epoxy and glass/epoxy under cyclic loading. They find very low damage rates after the first few cycles in graphite/epoxy even at about 90 percent of the failure level. For glass/epoxy, the AE data indicates that damage continued even when it was cycled at about 30 percent of the failure level. Laroche and Bunsell[8] used AE to obtain damage accumulation as a function of load holds at different levels for graphite/epoxy. They conclude on the basis of the AE data that the total damage sequence is independent of load history, but that the time to arrive at a given damage state depends on the load history. Lark and Moorhead[9] used AE to follow and characterize damage progression during sustained loading tests to failure of Kevlar/epoxy pressure vessels.

The above examples of how AE can give information on when, where, and how much damage occurs in composites demonstrate that AE can give unique information and insight into the development of damage functions. This information can take much of the guesswork out of determining the dependence of damage functions on variables such as load level, load cycling, time at load, materials, and strain rate. Approaches to determining this information without AE often must rely on very large numbers of samples with expensive and complicated experimental test plans or guesswork.

Application to Impact Studies

Ochiai *et al.*[10] correlated characteristics of the impact load vs. time curve with the corresponding AE during instrumented impact of plates of graphite/epoxy and sheet-molding compound. They demonstrate that with the proper choice of AE-system sensitivity, no AE is observed when no impact damage occurs and that AE is observed when damage does occur. This result led them to observe that with a fixed impact level, defective plates produce AE, and nondefective plates do not produce AE. Bailey *et al.*[11] show that AE can be used to detect prior impact damage in graphite/epoxy samples at low stress levels during subsequent tensile tests. These results indicate that AE can be a valuable tool to quickly study variables that influence impact damage in composites. AE provides new information on the impact-time-dependent damage-growth process just as instrumented impact gives us information relative to noninstrumented impact testing.

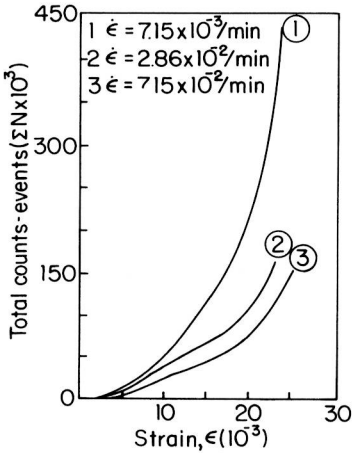

Fig. 1—Effects of strain rate on AE events in unidirectional E-glass/epoxy composite[4]

Application to Correlation of Damage with Stress/Strain Level

De Charentenay and Benzeggagh[12] and De Charentency *et al.*[13] demonstrate, using AE to monitor Mode I and Mode II delamination experiments, that it is possible to distinguish three separate stages of delamination: no cracking and initiation, microcracking, and stable growth and delamination (see Fig. 2). Old and Charlesworth[14] show that AE can be used to determine the stress level at which transverse cracks in Nb_3Sn fibers in a copper matrix began. Fuwa *et al.*[15] use AE information from monitoring of fiber bundles of graphite with no matrix, graphite/semicured matrix, and fully cured graphite/epoxy to develop a theory of failure for the composite. A number of investigators show a correspondence between a knee in the stress vs. strain curve and the start of AE or a change in the AE behavior (see Takehana and Kimpara,[16] Henneke and Herakovich,[17] and Kimpara *et al.*[18]).

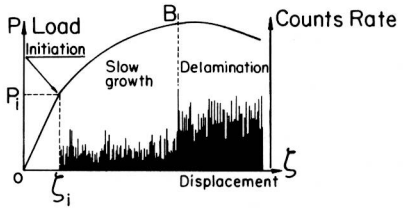

Fig. 2—AE during stages of Mode I delamination of glass/epoxy composite[3]

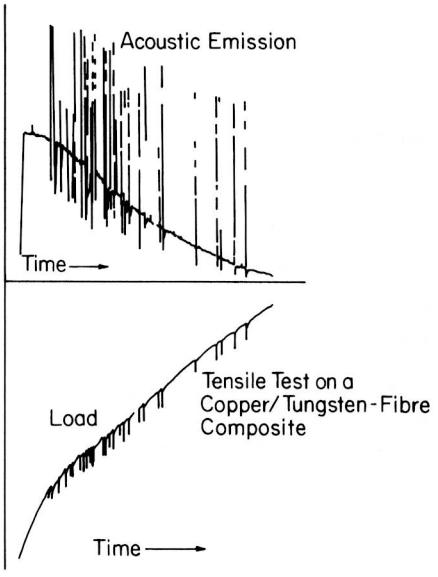

Fig. 3—Burst AE (from fiber fractures) and continuous AE (from matrix deformation) for a tensile test of a single tungsten fiber in a copper matrix[22]

Lloyd and Tangri[19] used AE to monitor fracture processes as a function of stress in a short fiber composite Mo/Al_2O_3. Mazzio *et al.*[20] used AE to keep track of graphite-fiber failures in model composites subjected to tensile loading after various thermal cycles. Harris *et al.*[21] show that during a tension test interrupted with load or displacement holds, when the test is resumed the damage pattern quickly goes back to that of a noninterrupted test. Swindlehurst[22] used AE monitoring for tension testing of a tungsten/copper composite to monitor stress levels for plastic flow of the copper matrix (by continuous AE) and fiber fractures (by AE bursts). (See Fig. 3.) Swanson and Hancock[23] used AE to distinguish when filament fracture began relative to plastic matrix flow for boron/aluminum unidirectional tension samples tested at 0 deg, 90 deg and 30 deg to the fiber axis. Grandemange and Street[24] used AE to determine the exact stress level of boron fiber failures in notched boron/aluminum fracture specimens. Rathbun *et al.*[25] used AE to experimentally determine the loading level above which glass/epoxy composite vessels suffered significant structural damage. Hutton[26] determined the stress level where fiber failures begin in nylon/polyurethane with AE monitoring.

The above results clearly demonstrate the great usefulness of AE data for the materials scientist. The ability to keep track of particular damage mechanisms as a function of stress or strain provides unique experimental input for development and correlation with theoretical work.

Application of Correlating AE With Other Measures of Damage

For interrupted tension tests of 0/90-deg glass/epoxy laminates, Sims *et al.*[27] correlate cumulative AE counts with increasing transverse crack area in the 90-deg plies (see Fig. 4), decreasing dynamic modulus, and increasing damping. Harris *et al.*[21] show a correlation of cumulative AE counts and changes in resonant frequency. Williams and Reifsnider[28] show that by monitoring AE (above 50 percent of the peak load) during fatigue of boron/aluminum and boron/epoxy samples with drilled holes that a good correlation of the cumulative total of AE counts and the compliance change is obtained. This result leads them to conclude that the same physical mechanism which causes the AE also causes the compliance change.

The above results again demonstrate a unique role for AE data: AE can provide the reason and characterize the growth of damage that leads to changes in other measured properties of composites.

Application to Cure Studies

Phillips and Harris[29] compare the AE during subsequent tensile tests for chopped strand mat/polyester cured at two different temperatures. They found about two times as many AE events for the composites cured at the higher temperature which results in a more brittle matrix. Hinton *et al.*[30] used AE to monitor the cure process of flat laminates of both Kevlar and glass. They believe the first AE in the cure cycle is due to outgassing of the resin and that the later activity is caused by cure shrinkage of the resin relative to the fiber. They observed higher amplitudes of AE and more AE events in Kevlar composites compared to glass composites. Houghton *et al.*[31] used AE to monitor cure cool-down of E-glass/epoxy. They found that a fast cool-down from peak temperature led to large and frequent AE bursts while a slow cool-down resulted in small and infrequent AE, as well as a slightly lower tensile strength (see Fig. 5).

Again AE provides unique data to the person studying the effects of cure cycles. Monitoring the cure process provides immediate information that could result in an improved composite with lower residual stresses and less residual damage.

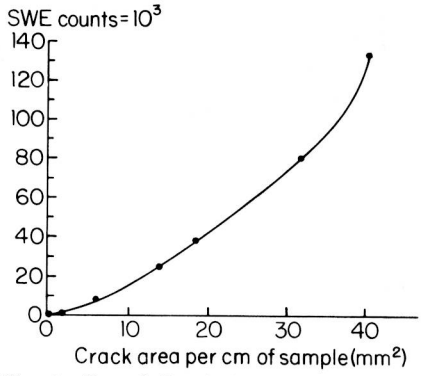

Fig. 4—Correlation between summation of AE and transverse crack area for tensile test of a 0-deg/90-deg glass/epoxy laminate[27]

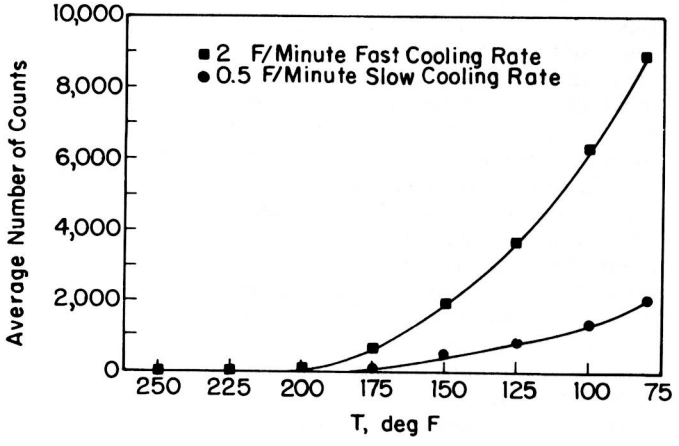

Fig. 5—The effect of rate of cooldown during cure of E-glass/epoxy laminate[31]

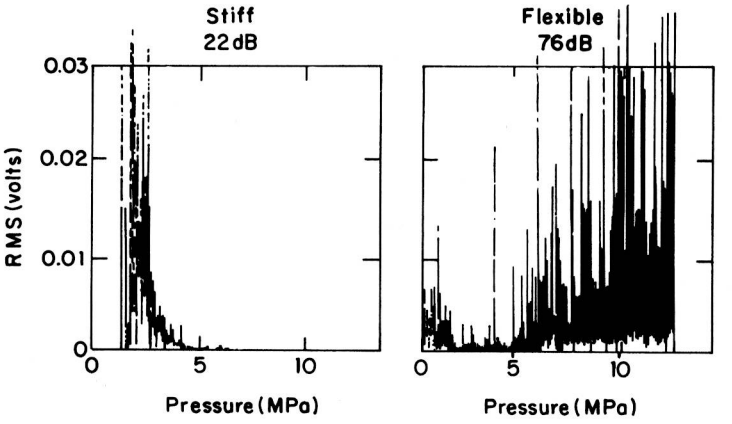

Fig. 6—AE shows dramatic differences in damage accumulation with flexible vs. stiff epoxies in Kevlar 49/epoxy vessels[34]

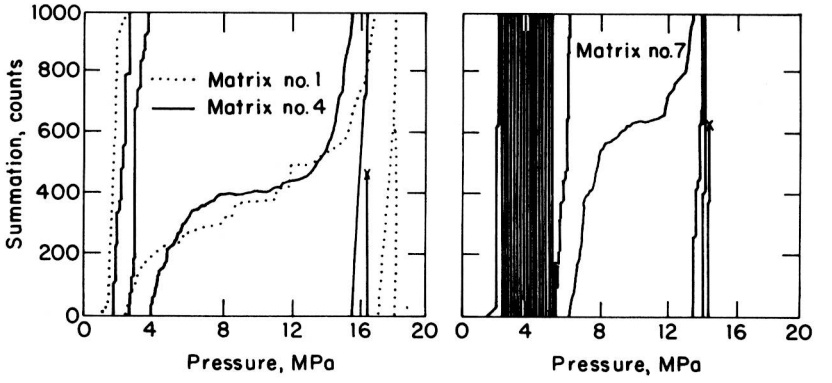

Fig. 7—Early AE for Kevlar 49/epoxy with different resins has an inverse correlation with average failure levels. Average failure levels: No. 1—18.3 MPa, No. 4—16.0 MPa, No. 7—14.8 MPa[37]

Application to Differences in Matrix Materials

McGarry *et al.*[32] used audible AE to show the reduction in matrix cracks when increasing amounts of liquid rubber were added to the polyester matrix. As the fracture properties improved, the AE from the matrix-cracking source mechanism decreased substantially. Hamstad and Chiao[33] show for both Kevlar and graphite pressure vessels that the AE begins at a higher pressure for less rigid epoxies. Later, Hamstad[34] shows for Kevlar/epoxy pressure vessels that a flexible high-elongation epoxy system results in the disappearance of the high-amplitude early AE peak which occurs for stiff and low-elongation epoxy systems (see Fig. 6). He also shows that when the pressure vessels with the stiff epoxy system are tested at an elevated temperature where the epoxy becomes flexible that the early peak again disappears. Norwood and Millman[35] show, based on AE data, that the strain to first matrix damage (i.e., initiation of AE) is greater for more flexible resin systems in glass-reinforced polyester under tensile loading of samples. Hamstad and Chiao[36,37] show that the amount of early AE in Kevlar/epoxy cylindrical pressure vessels can be used as an indicator of the dependence of burst strength on the choice of matrix material (see Fig. 7).

These results demonstrate that AE can be used to confirm proposed damage mechanisms and to study how these mechanisms can be changed by matrix modification.

Application to Differences in Second Phase (Usually Fibers)

Holt and Worthington[38] show for tensile tests of unidirectional samples that glass/epoxy results in the generation of much more AE than graphite does with the same epoxy system. They also observe that the graphite/epoxy system fails without showing the same warning of impending failure which the glass/epoxy shows. Fuwa *et al.*[39] earlier had reported this lack of warning for graphite/epoxy rings and pressure vessels. Grenis and Levitt[40] observed for boron/aluminum that the unidirectional composite goes to failure much more gradually with many more total AE counts than graphite/aluminum does even though in a given cross section there are a lot less boron fibers than graphite fibers due to the larger diameter of the boron fibers. Crump and Droge[41] studied the effect of increased glass content under tensile testing. They found that large amplitude events occur at a lower percentage of the failure stress and the summation-of-counts curve exponentially increases at a lower percentage of the failure stress as the glass content increases (see Fig. 8). Bunsell *et al.*[42] show by measuring the AE energy at fiber failure of Kevlar, glass, and graphite that Kevlar fibers fail by a different mechanism than the other two fibers. Hamstad and Chiao[33] show with AE that graphite/epoxy cylindrical pressure vessels fail in a very brittle fashion compared to Kevlar/ or glass/epoxy vessels. Arrington and Harris[43] used AE to study changes in a hybrid com-